Article

$^{229}ThF_4$ thin films for solid-state nuclear clocks

https://doi.org/10.1038/s41586-024-08256-5

Received: 25 July 2024

Accepted: 21 October 2024

Published online: 18 December 2024

Check for updates

Chuankun Zhang[1], Lars von der Wense[1,9], Jack F. Doyle[1], Jacob S. Higgins[1], Tian Ooi[1], Hans U. Friebel[1,10], Jun Ye[1]✉, R. Elwell[2], J. E. S. Terhune[2], H. W. T. Morgan[3,4], A. N. Alexandrova[3], H. B. Tran Tan[5,6], Andrei Derevianko[5] & Eric R. Hudson[2,7,8]✉

After nearly 50 years of searching, the vacuum ultraviolet ^{229}Th nuclear isomeric transition has recently been directly laser excited[1,2] and measured with high spectroscopic precision[3]. Nuclear clocks based on this transition are expected to be more robust[4,5] than and may outperform[6,7] current optical atomic clocks. These clocks also promise sensitive tests for new physics beyond the standard model[5,8–12]. In light of these important advances and applications, a substantial increase in the need for ^{229}Th spectroscopy targets in several platforms is anticipated. However, the growth and handling of high-concentration ^{229}Th-doped crystals[5] used in previous measurements[1–3,13,14] are challenging because of the scarcity and radioactivity of the ^{229}Th material. Here we demonstrate a potentially scalable solution to these problems by performing laser excitation of the nuclear transition in $^{229}ThF_4$ thin films grown using a physical vapour deposition process, consuming only micrograms of ^{229}Th material. The $^{229}ThF_4$ thin films are intrinsically compatible with photonics platforms and nanofabrication tools for integration with laser sources and detectors, paving the way for an integrated and field-deployable solid-state nuclear clock with radioactivity up to three orders of magnitude smaller than typical ^{229}Th-doped crystals[1–3,13]. The high nuclear emitter density in $^{229}ThF_4$ also potentially enables quantum optics studies in a new regime. Finally, we present the estimation of the performance of a nuclear clock based on a defect-free ThF_4 crystal.

The ^{229}Th nucleus has been the subject of extensive scientific research for several decades, as it possesses a remarkable low-energy isomeric nuclear transition at about 8.4 eV. This feature enables precision laser spectroscopy and has led to proposals for several important applications[5,15,16], including the development of a nuclear optical clock[17–19]. Of particular interest, a solid-state nuclear clock[4,5,20] can be constructed by tightly confining the nuclei in a high-bandgap crystalline lattice. This confinement enables laser-based, recoil-free Mössbauer spectroscopy without sophisticated laser cooling and trapping techniques. Owing to small nuclear electromagnetic moments, the nuclear clock transition frequency remains relatively insensitive to external perturbations in the crystalline host. Probing macroscopic amounts (>10^{12}) of ^{229}Th atoms in a solid promises excellent counting statistics and good clock stability. An optical clock based on such a solid-state ^{229}Th sample is thus highly desirable for field applications because of its potential robustness and simplicity.

Recently, rapid progress has been made in this field. Direct laser excitation and measurement of the nuclear clock transition[1,2] were demonstrated; subsequently, high-precision spectroscopy referenced to the ^{87}Sr clock[3] was performed using a vacuum ultraviolet (VUV) frequency comb to determine the transition frequency to the 10^{-12} level. These experiments lay the foundation for a solid-state nuclear clock based on ^{229}Th doped into high-bandgap crystals. However, the scarcity and the radioactivity of ^{229}Th complicate the crystal growth process. ^{229}Th is a controlled material that does not naturally exist, cannot be produced conveniently and is already in high demand for medical research[21]. Although the estimated world stock of ^{229}Th with reasonable isotopic purity is 40 g (ref. 22), most of it is mixed with other chemical elements such as ^{233}U and is thus not readily available. The amount of ^{229}Th available to researchers is typically limited to at most a few milligrams, necessitating challenging miniaturized crystal growing techniques[13,23–25] to obtain crystals with sufficient ^{229}Th dopant density. Furthermore, given that cutting and polishing techniques require crystals with dimensions on the millimetre scale, these crystals typically have a radioactivity of ≳10 kBq. This level of radioactivity requires appropriate radiation safety precautions and limits the proliferation of nuclear clocks.

An alternative to crystal growth is physical vapour deposition (PVD), in which the desired material is evaporated from a hot crucible and subsequently condensed onto a substrate. PVD is frequently used to produce radioactive targets[26–31], mainly for accelerator facilities. As $^{232}ThF_4$ thin films with the naturally abundant isotope are routinely used in optics, PVD of $^{232}ThF_4$ is a mature technology[32]. However, PVD of $^{229}ThF_4$ is much less developed with, to the best of our knowledge, only one brief description in the literature[28]. Here we report the fabrication of thin film $^{229}ThF_4$ targets (30–100 nm thickness) by miniaturized radioactive PVD on various substrates such as Al_2O_3 and MgF_2. We fabricate targets as small as 50 μm diameter using only micrograms of ^{229}Th material, orders of magnitude smaller than that needed for a

[1]JILA, NIST and University of Colorado, Department of Physics, University of Colorado, Boulder, CO, USA. [2]Department of Physics and Astronomy, University of California, Los Angeles, CA, USA. [3]Department of Chemistry and Biochemistry, University of California, Los Angeles, Los Angeles, CA, USA. [4]Department of Chemistry, University of Manchester, Manchester, UK. [5]Department of Physics, University of Nevada, Reno, NV, USA. [6]Los Alamos National Laboratory, Los Alamos, NM, USA. [7]Challenge Institute for Quantum Computation, University of California Los Angeles, Los Angeles, CA, USA. [8]Center for Quantum Science and Engineering, University of California Los Angeles, Los Angeles, CA, USA. [9]Present address: Johannes Gutenberg-Universität Mainz, Institut für Physik, Mainz, Germany. [10]Present address: Independent researcher, Wörth, Germany. ✉e-mail: ye@jila.colorado.edu; eric.hudson@ucla.edu

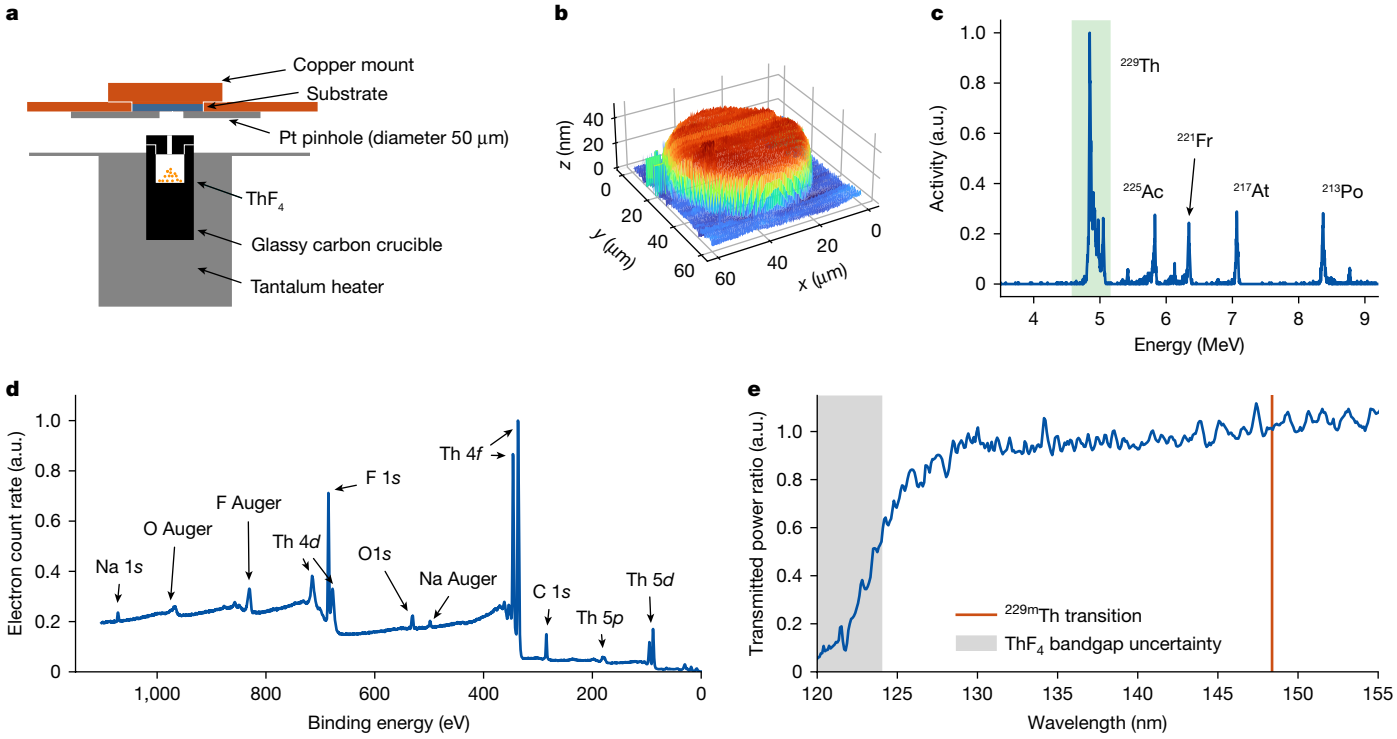

Fig. 1 | $^{229}ThF_4$ target fabrication procedure and characterization. **a**, Schematic of the $^{229}ThF_4$ target vapour deposition setup. A small amount (<10 µg) of $^{229}ThF_4$ is loaded into a glassy carbon crucible for radioactive PVD. On heating, $^{229}ThF_4$ vapour effuses from a small (about 1 mm diameter) hole in the crucible and deposits on a nearby substrate (about 3 mm away), forming about a 5 mm diameter round target. An optional Pt mask is used to generate a small-area target with the desired shape. **b**, Spatial profile of a small $^{229}ThF_4$ target measured using AFM. The target is a disk of about 50 µm diameter and around 30 nm thickness. **c**, Alpha spectrum of the small-area target as shown in **b**. Peaks in the green highlighted region (4.59–5.15 MeV) come from ^{229}Th, corresponding to a ^{229}Th activity of about 3 Bq. **d**, Chemical composition of a similarly fabricated, about 5 mm diameter, $^{229}ThF_4$ target measured with XPS. Peaks corresponding to each specific element are annotated[58]. This confirms that the chemical composition of the thin film is ThF_4. **e**, VUV transmission of a similarly fabricated ThF_4 thin film of about 1 µm thickness. The ratio of the transmitted VUV power between the ThF_4 coated and uncoated areas on a MgF_2 substrate is plotted, confirming the VUV transparency down to the measured ThF_4 bandgap of 10.2(2) eV (shaded grey) in ref. 36 and in agreement with the results reported in ref. 32. a.u., arbitrary units.

single-crystal growth batch[13,23–25]. By reducing the target area without sacrificing the target optical density, the 50 µm target has three orders of magnitude smaller radioactivity than typical ^{229}Th-doped crystals, corresponding to a much reduced radioactive hazard[33] and thus vastly relaxed safety measures.

Although ThF_4 was originally assumed to have a band gap below the 8.4 eV ^{229}Th isomer energy[34] and, therefore, not considered a suitable host for a solid-state nuclear clock[23,25], recent work[35,36] indicates that the band gap is roughly 10 eV. Very recently, photoluminescence and radioluminescence of $^{232}ThF_4$ thin films were measured[37], highlighting a low fluorescence background that is beneficial for nuclear clock operation. This suggests the possibility of observing the radiative decay of the ^{229}Th nuclear clock isomer in $^{229}ThF_4$. To confirm this, we perform nuclear laser spectroscopy on PVD $^{229}ThF_4$ films using a VUV laser system. We observe a single spectroscopic line at $2020406.8(4)_{stat}(30)_{sys}$ GHz for a $^{229}ThF_4$ target on a MgF_2 substrate and at $2020409.1(7)_{stat}(30)_{sys}$ GHz for a Al_2O_3 substrate, which we assign to the ^{229}Th nuclear isomeric transition based on the previous crystal results[1–3]. The numbers in parentheses denote 68% confidence intervals. The measured lifetimes in these samples, $150(15)_{stat}(5)_{sys}$ s on Al_2O_3 and $153(9)_{stat}(7)_{sys}$ s on MgF_2, are identical within error and are substantially shorter than that observed in ^{229}Th:CaF_2 (τ = 641(4) s; ref. 3) and ^{229}Th:LiSrAlF$_6$ ($\tau = 568(13)_{stat}(20)_{sys}$ s; ref. 2) crystals.

The demonstrated fabrication of $^{229}ThF_4$ thin film targets with thicknesses of 30–100 nm and diameter of 50 µm–5 mm and the ensuing observation of the nuclear clock transition therein show a pathway towards a future integrated low-radioactivity solid-state nuclear clock that can be fabricated with existing thin film coating technology. In what follows, we describe the $^{229}ThF_4$ target fabrication procedure and characterization, the laser spectroscopy apparatus and results, and then discuss the advantage of $^{229}ThF_4$ films or ^{229}Th-doped ThF_4 crystals in a solid-state nuclear optical clock.

Miniaturized PVD of $^{229}ThF_4$

The vapour deposition setup is shown in Fig. 1a. We start with the ^{229}Th in dry nitrate form, $Th(NO_3)_4$, purchased from the National Isotope Development Center. We dissolve the nitrate in ultrapure water for easy handling of microscopic quantities using adjustable volume micropipettes. We directly load the desired quantity of $Th(NO_3)_4$ solution into a glassy carbon crucible and add excess HF to obtain $^{229}ThF_4$ precipitate, weighing only a few micrograms, which is otherwise impractical to handle. The leftover aqueous solution of HF and HNO_3 is then evaporated in a fume hood at elevated temperatures.

After initial material loading, a crucible cap is installed to further decrease the solid angle of the evaporation beam. The crucible is heated using a tantalum heater to above 1,000 °C in 10^{-6} mbar vacuum to vaporize the $^{229}ThF_4$ onto a substrate 3 mm away, forming a non-uniform coating of about 5 mm in diameter. During the coating run, we do not actively control the substrate temperature. The thickness of this large-area coating is measured with a stylus profilometer. The centre thickness is typically 30–100 nm, about twice that of the edges, depending on the material amount used in the coating run. The fabricated thin film coatings are likely amorphous (Methods).

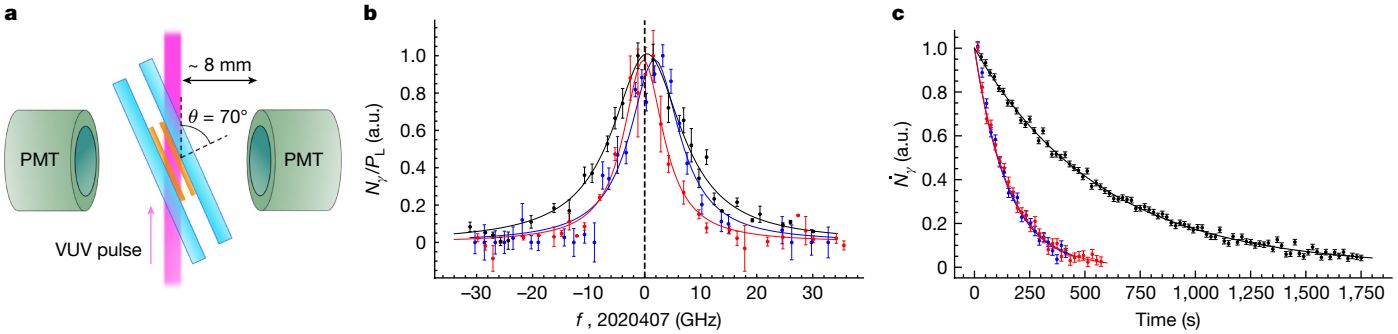

Fig. 2 | Nuclear spectroscopy of the ^{229}Th clock transition in the $^{229}ThF_4$ film. **a**, Schematic of the $^{229}ThF_4$ target region. Note that the beam is at 70° with the normal of the two plates to maximize the effective illumination area. The plates are held with a gap of about 1 mm between them. **b**, Recorded nuclear fluorescence normalized by laser power versus VUV laser frequency. The observed power-normalized fluorescence for the $^{229}ThF_4$ film on a Al_2O_3 (MgF_2) substrate is shown in blue (red). All error bars represent the standard error of the mean. **c**, Recorded nuclear fluorescence rate $\dot{N}_\gamma$ normalized by laser power versus time after the laser is extinguished. The observed radiative decay for $^{229}ThF_4$ on a Al_2O_3 (MgF_2) substrate is shown in blue (red). In both **b** and **c**, the peaks of all curves were normalized to unity and the corresponding result observed in ^{229}Th:$LiSrAlF_6$ (ref. 2) is shown in black for comparison. a.u., arbitrary units.

To fabricate small-area targets and minimize the ^{229}Th consumption, Pt masks with laser-drilled pinholes are used. As Pt has a higher evaporation temperature and is chemically inert, the $^{229}ThF_4$ material deposited on the Pt mask can be recycled for future coating runs. The substrate and optional pinholes are held in place by a copper mounting structure (Fig. 1a).

The physical dimensions of one small target, fabricated on a Pt-coated silicon wafer substrate, are measured using an atomic force microscope (AFM) and shown in Fig. 1b. To demonstrate the ability for customizing target size and shape, we fabricated an approximately 50 µm diameter target using a Pt mask with the same dimensions. With a thickness of about 30 nm, the volume of the $^{229}ThF_4$ corresponds to roughly 7×10^{11} atoms or an activity of about 2 Bq. Alpha spectroscopy of the target using a calibrated alpha spectrometer, shown in Fig. 1c, confirms the presence of ^{229}Th and its daughter isotopes. We extract a ^{229}Th activity of about 3 Bq from the alpha spectrum, in rough agreement with the estimation from the target volume, by integrating over the region of interest corresponding to the ^{229}Th alpha peaks (Fig. 1c, green shaded area).

The chemical composition of the thin film is characterized by X-ray photoelectron spectroscopy (XPS) as shown in Fig. 1d, which confirms the main constituents of the film as thorium and fluorine. Without a detailed analysis of the uncertainties, we extract the atom number percentages from the XPS spectrum to be 19.4% thorium, 36.6% fluorine, 34.2% carbon, 8.4% oxygen and 1.4% sodium. The oxygen and carbon composition presumably originates from hydrocarbon contamination because of air exposure. A subsequent XPS measurement on a similar $^{232}ThF_4$ film (not shown) is performed after the removal of the top layer by in situ argon sputtering. We observe that the peak corresponding to carbon 1*s* disappears and the oxygen 1*s* peak decreases markedly, in agreement with this hypothesis. The sodium peak probably comes from trace contamination in the water used during the coating process.

The optical property of the thin film is characterized by measuring the transmitted VUV power ratio between a coated and uncoated sections of a single MgF_2 substrate using a D_2 lamp and a grating spectrometer. The result is shown in Fig. 1e, in which the ^{229}Th isomer transition wavelength is indicated by the orange line. The spectral transmission agrees qualitatively with the ThF_4 measurement reported in ref. 32, demonstrating high VUV transmission. These data are consistent with the >10 eV ThF_4 bandgap predicted in ref. 35 and measured in ref. 36, as indicated by the grey-shaded area. Based on the large bandgap, we expect that the host quenching effects such as internal conversion will not dominate the relaxation of the nuclear clock state, providing the opportunity for radiative fluorescence detection.

Nuclear laser spectroscopy

Using this miniaturized PVD apparatus, two types of large-area $^{229}ThF_4$ targets (each approximately 21 kBq in activity) for the nuclear laser spectroscopy were fabricated on VUV-transparent Al_2O_3 and MgF_2 substrates. We performed a coating run for each target with two identical substrates placed side by side, producing two semicircular $^{229}ThF_4$ films. The semicircular $^{229}ThF_4$ films are around 2.5 mm in radius and about 30 nm in average thickness. The substrate dimensions are about 8 mm × 4 mm × d, where d = 175 µm for Al_2O_3 and 250 µm for the MgF_2. Two identical $^{229}ThF_4$ films with the same substrate material are placed facing each other with about 1 mm gap between them, forming one target used in the experiment. This sandwich configuration was chosen to minimize radioactive contamination of the vacuum chamber from recoil daughter nuclei on ^{229}Th alpha decay.

Using the system described in refs. 2,23, VUV radiation was produced by resonance-enhanced four-wave mixing of two pulsed dye lasers in Xe gas. The frequency of the first pulsed dye laser, ω_u, was locked to the $5p^6\,{}^1S_0 \rightarrow 5p^5\left({}^2P^\circ_{3/2}\right) 6p^2[1/2]_0$ two-photon transition of Xe at about 249.63 nm. The frequency of the second pulsed dye laser, ω_v, was scanned to produce VUV radiation in the Xe cell given by the difference mixing relation $\omega = 2\omega_u - \omega_v$. All three laser beams then impinge off-axis with respect to a MgF_2 lens, whose chromatic dispersion is used with downstream pinholes to spatially filter the VUV beam and pass it towards the $^{229}ThF_4$ samples. The laser system delivers 30 pulses per second to the crystal with a typical VUV pulse energy of about 2 µJ per pulse (see refs. 2,23 for details).

The $^{229}ThF_4$ samples were mounted in a vacuum chamber with two VUV-sensitive photomultiplier tubes (Hamamatsu R6835 PMTs) and a pneumatic shutter system (not shown) to protect the PMTs from direct exposure to the VUV laser (Fig. 2a). The PMTs are operated in a cathode-grounded configuration, and their output waveforms recorded by a 1 Gs s^{-1} waveform digitizer (CAEN DT5751) for subsequent post-processing. The VUV laser irradiates the samples at approximately 70° from the direction normal to the plates to increase the effective illumination volume. We terminate the laser beam on a custom VUV energy detector. The vacuum chamber is maintained with an Ar atmosphere at a pressure of about 10^{-2} mbar to provide high VUV transmission while minimizing degradation of optics because of hydrocarbon deposition[23].

We observe the nuclear transition by monitoring the fluorescence from the $^{229}ThF_4$ film following the VUV laser illumination. Using this system, nuclear spectroscopy of the ^{229}Th clock transition in the $^{229}ThF_4$ film was recorded (Fig. 2b). We observe a single spectroscopic feature at $2020406.8(4)_{stat}(30)_{sys}$ GHz for the $^{229}ThF_4$ film on the MgF_2

substrate and at 2020409.1(7)$_{stat}$(30)$_{sys}$ GHz for the $^{229}ThF_4$ film on the Al_2O_3 substrate. For these measurements, the $^{229}ThF_4$ was illuminated by the VUV laser for approximately 450 s, the shutters opened in about 100 ms, and the resulting fluorescence was recorded for roughly 450 s. Each data point represents an average of the number of photons detected above the background in both PMTs and normalized by the total laser power. The Al_2O_3 sample exhibited a lower signal-to-noise ratio because of an increased radioluminescence background; thus, each point was typically repeated around three times. The spectra recorded in ^{229}Th:LiSrAlF$_6$ are shown for reference in Fig. 2b as black points (ref. 2). The laser bandwidth is estimated to be about 10 GHz and dominates the linewidth of the observed spectral features. The smaller spectral linewidth observed in the $^{229}ThF_4$ samples compared with the ^{229}Th:LiSrAlF$_6$ sample is attributed to a decrease in laser drift during data collection because of the shorter excitation time here (450 s) compared with ref. 2 (1,800 s). The systematic uncertainty of the measurements is dominated by wave meter calibration[2].

The expected amount of fluorescence is calculated from detailed analysis of the detection efficiency of our system (Methods), the known thorium density and thickness of the $^{229}ThF_4$ film, and the measured laser parameters, and is found to be considerably larger (about 10^3 times) than the experimental observation. As detailed in ref. 2, the hyperfine interaction couples the nuclear degree of freedom with the electronic degree of freedom. If there are electronic states with excitations at or below the nuclear energy because of defects in the local crystal structure, for example, quenching of the nuclear transition is possible and a reduced fraction p of the ^{229}Th participates in the narrow nuclear fluorescence. From the observed signals, we find the estimated emitter fraction as $p = 2(1) \times 10^{-3}$ for both targets, assuming about 2 μJ per pulse.

Using the same system, the lifetime of the isomeric transition was measured by collecting the fluorescence as a function of time after laser excitation (Fig. 2c) and found to be 150(15)$_{stat}$(5)$_{sys}$ s on Al_2O_3 and 153(9)$_{stat}$(7)$_{sys}$ s on MgF_2. Here, the systematic error is estimated based on the observed drifts in background count rates because of the thermal instability of the PMT gain. These lifetimes are markedly shorter than the value previously observed in ^{229}Th:CaF_2 (τ = 641(4) s; ref. 3) and ^{229}Th:LiSrAlF$_6$ (τ = 568(13)$_{stat}$(20)$_{sys}$ s; ref. 2) crystals.

This shortened lifetime is sufficient and perhaps even beneficial for nuclear clock operation. In the Methods, we consider several mechanisms of lifetime shortening, including the Purcell[38] and superradiance effects[39,40]. We conclude that the observed shorter isomer lifetime in $^{229}ThF_4$ films is likely because of two main factors: a high refractive index of $^{229}ThF_4$ and potential quenching effects by the host material. Although the refractive index required to fully explain the lifetime (n = 2.2–2.5) may be higher than our estimate ($n \approx 1.95(30)$), an additional nuclear decay mechanism can arise from a combination of hyperfine mixing of nuclear and electronic states and the hybridization of electronic states because of crystal fields[2]. The quenching rate could be further enhanced in thin films such as $^{229}ThF_4$ because of modified electronic levels[41] arising from mechanical strain and film–substrate interface effects such as lattice mismatch strains and dipole layer formation at the interface[42,43]. Other quenching effects from electronic states could arise from the potentially amorphous structure or trace contaminants.

These results make it clear that ^{229}Th nuclear isomeric transition can be driven and observed in $^{229}ThF_4$ thin films and potentially even bulk crystals. This opens many possibilities as ThF_4 film growth is well-developed, for example, for optical coatings—that is, ^{229}Th can be directly incorporated in optical components such as mirrors, lenses and waveguides. In what follows, we analyse the expected performance of a $^{229}ThF_4$-based nuclear clock.

Projected $^{229}ThF_4$ clock performance

Although the crystallinity of the fabricated $^{229}ThF_4$ thin films needs to be characterized (Methods) and possibly improved[44] in future

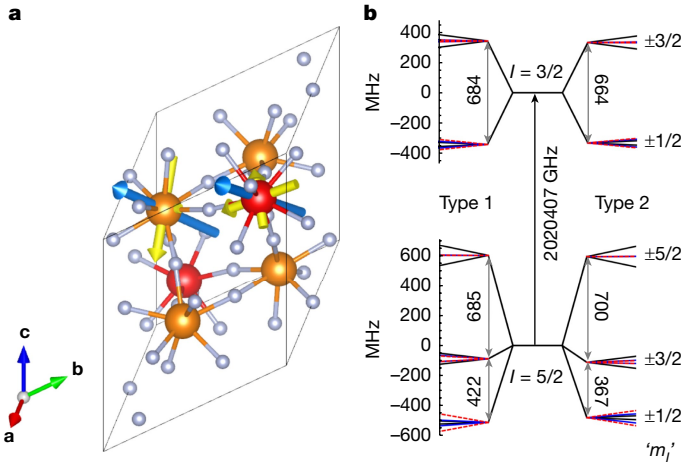

Fig. 3 | Projected clock performance of $^{229}ThF_4$. a, Unit cell of ThF_4 showing the EFG eigenvectors. Thorium atoms are shown as red and orange spheres, the two colours denoting the two inequivalent crystallographic positions, and fluorine atoms are shown in grey. The light blue vectors show the largest diagonal EFG components, V_{zz}, and the yellow vectors show the minor components, V_{xx} and V_{yy}. The lengths of the vectors are proportional to the EFG magnitudes along the respective directions. **b**, Numerically calculated EFG and Zeeman splittings in the two inequivalent thorium sites. The Zeeman shift from 0 T to 10 T is plotted for a magnetic field along the $\hat{x}$ (blue), $\hat{y}$ (red, dashed) and $\hat{z}$ (black) directions.

experiments, it is well known that ThF_4 single crystals[45] can be grown. Therefore, we perform density functional theory (DFT) calculations (Methods) using the monoclinic crystal structure of ThF_4, space group $C2/c$ (number 15) (ref. 46), (Fig. 3a) in which the thorium atoms are nominally in the $^{229}Th^{4+}$ charge state. The main effect of the crystal on the $^{229}Th^{4+}$ nucleus is the coupling of the ^{229}Th nuclear electric quadrupole (EQ) moment to the crystal electric field gradients (EFGs) $\{V_{xx}, V_{yy}, V_{zz}\}$ and the coupling of the ^{229}Th nuclear magnetic moment to the magnetic field created by the other atoms in the crystal[5]. $^{229}ThF_4$ is an ionic crystal with no unpaired electrons; therefore, the magnetic field experienced by a ^{229}Th atom comes from the other nuclear magnetic moments in the crystal. Thus, the nuclear energy levels are described by the Hamiltonian:

$$\hat{H} = -\mu_\alpha \mathbf{I}\cdot\mathbf{B} + \frac{eQ_\alpha V_{zz}}{4I(2I-1)}[3\hat{I}_z^2 - \hat{I}^2 + \eta(\hat{I}_x^2 - \hat{I}_y^2)], \quad (1)$$

where $\hat{I}$ is the total nuclear spin operator, $\hat{I}_{x,y,z}$ are the components of the nuclear spin operators, $\eta = |V_{xx} - V_{yy}|/V_{zz}$ is the EFG asymmetry parameter with the choice $|V_{zz}| > |V_{xx}| > |V_{yy}|$ and $\alpha = \{g, e\}$ denotes the ground and excited nuclear states, respectively, which is parameterized by Q_g = 3.149(4) eb (ref. 47), $\mu_g = 0.360(7)\mu_N$ (refs. 48,49), Q_e = 1.77(2) eb (refs. 50,51) and $\mu_e = -0.378(8)\mu_N$ (refs. 50,51), where μ_N is the nuclear magneton and eb stands for electron-barn.

In contrast to the ^{229}Th-doped high-bandgap crystals previously considered[25,52,53], ThF_4 is expected to host ^{229}Th in two non-equivalent sites[46]. The first site (type 1), shown as orange spheres in Fig. 3a, experiences a crystal EFG of $V_{zz} = 310.5$ V Å^{-2} and $\eta = 0.437$ and is twice as populated as the second site (type 2), shown as red spheres in Fig. 3a, which experiences a crystal EFG of $V_{zz} = 308.9$ V Å^{-2} and $\eta = 0.194$.

Owing to the differing EFGs, these two sites have non-degenerate energy levels (Fig. 3b) and therefore distinct laser spectra. Having control of two separate populations of ^{229}Th nuclei in this crystal enables several new experiments, including the study of spin exchange interactions between thorium nuclei, and could be used to improve the performance of a nuclear clock as these populations can be independently probed, thereby reducing the Dick effect[54].

The main source of inhomogeneous broadening of the nuclear clock transitions is the magnetic dipole–dipole interaction between the ^{229}Th nuclei and the nearby ^{19}F nuclei. Using the positions found for the ^{229}Th and ^{19}F atoms from the DFT calculation, the magnetic moments of the nuclei and the assumption that the nuclear spins are oriented randomly, we estimate that the magnetic field seen by a thorium nucleus fluctuates with a standard deviation of approximately 5 G. Thus, the Zeeman interaction broadens the levels by an amount of order 1–10 kHz, with the transition linewidth given by the relative Zeeman shift of the states involved in the clock transition. At first glance, because the magnetic moment of the ^{229}Th isomeric state is nearly equal but opposite to that of the nuclear ground state, a clock based on, for example, either of the $|I = 5/2, m_I = \pm 1/2\rangle \leftrightarrow |3/2, \mp 1/2\rangle$ transitions would exhibit a magnetic field sensitivity of only $0.009(5)\mu_N = 7(4)$ Hz G^{-1}, leading to a broadening of $\lesssim$100 Hz. However, because the EFG orients the nucleus, the Zeeman sensitivity depends strongly on the direction of the magnetic field relative to the EFG axes, as shown in Fig. 3b, in which the Zeeman shift from 0 T to 10 T is plotted for a magnetic field along the $\hat{x}$ (blue), $\hat{y}$ (red, dashed) and $\hat{z}$ (black) directions. The energy levels are labelled by the m_I quantum number of the primary component of the eigenstate. The alignment of the quadrupole moment, and therefore the nuclear spin and magnetic moment to the EFG $\hat{z}$-axis, results in an increased sensitivity of stretched states to magnetic fields along the $\hat{z}$-axis and a decreased sensitivity of stretched states to magnetic fields along the $\hat{x}$- and $\hat{y}$-axes. This markedly alters the Zeeman sensitivity of the available nuclear transitions. By numerically diagonalizing the Hamiltonian for a sample of magnetic fields (Methods), the Zeeman-limited linewidths of the various transitions are estimated to be approximately 1–7 kHz, with the least broadening of about 1.1 kHz realized by the $|5/2, \pm 1/2\rangle \leftrightarrow |3/2, \mp 1/2\rangle$ transition for type 2 sites. This increased Zeeman sensitivity as compared with a free ^{229}Th nucleus highlights the part the EFG plays in determining clock performance and suggests that a crystal structure with vanishing EFG, as would occur if ^{229}Th was positioned in a site of cubic symmetry, could lead to improved performance.

Because the quantization axis is set by the crystal EFG, selecting a nuclear transition with improved magnetic field performance requires light of specific polarization propagating in a direction set by the crystal EFG. This is straightforward in a single crystal of $^{229}ThF_4$ but may be more difficult to achieve in ^{229}Th:LiSrAlF$_6$ (refs. 2,5) and ^{229}Th:CaF$_2$ (ref. 1) because the symmetry axis of the EFG depends on the geometry of the interstitial ^{19}F atoms required for charge compensation.

With these calculations, the performance of a $^{229}ThF_4$ thin film nuclear clock can be estimated. Assuming a 100-nm thick film, a probe laser linewidth much smaller than the inhomogeneous Zeeman-limited transition linewidth and a probe laser power of 1 μW, the performance of a clock based on the $|5/2, \pm 1/2\rangle \leftrightarrow |3/2, \mp 1/2\rangle$ transition is estimated to have a fractional instability of 5×10^{-17} at 1*s* for both type 1 and type 2 sites (Methods). Estimating the inaccuracy is not yet possible for these systems and will be the subject of future work; however, strain and temperature sensitivity[5] can be expected as important systematics.

Discussion and outlook

Apart from precision measurement applications, the vapour-deposited $^{229}ThF_4$ thin films with controllable thickness also provides a new platform for studying Purcell effects. We expect that when the film thickness is comparable to or smaller than the excitation wavelength, the film thickness and substrate refractive index can be exploited to control the emitter lifetime and emission direction. These effects can potentially be used for engineering new quantum optics devices or improving the nuclear clock performance.

Although superradiant effects are not observed in this work because of the inhomogeneous broadening and low participation factor, the emitter number in a cubic wavelength for $^{229}ThF_4$, $(\lambda/n_{ThF_4})^3\rho_{Th} > 10^6$, is more than three orders of magnitude higher than that achieved in ^{229}Th-doped crystals. Using $^{229}ThF_4$ waveguides or resonators for increased optical density, a new regime for quantum optics studies involving nuclear superradiance[55] and coherent nuclear forward scattering[40] seems accessible in $^{229}ThF_4$.

With this demonstration of nuclear spectroscopy in $^{229}ThF_4$ thin films, we also rekindle the interest of the community in ThF_4 crystals. Doping ^{229}Th in ThF_4 does not create defects or alter the crystal structure. This uniquely enables control over the crystal EFG quantization axis for polarization-selective excitation of the clock states. Furthermore, in ^{229}Th-doped thin film or crystalline ThF_4 samples, we can tune the emitter density by changing the doping concentration for precision measurement and quantum optics studies. Moreover, ThF_4 multilayer coatings have been used regularly in industrial applications, providing opportunities for scalable production of solid-state nuclear clocks based on integrated ThF_4 photonic structures that can be incorporated with VUV lasers and detection systems.

As the observed participation fraction of the nuclear transition in optical decay is low (about 10^{-3}), it is necessary to continue investigating the underlying quenching mechanism and methods for improvement. Narrow, state-resolved nuclear transitions[3] in the fabricated thin films have not yet been observed because of the low participation fraction and potentially also inhomogeneous line-broadening effects caused by the amorphous characteristics of the sample. Annealing and fluorination processes may greatly increase the participation fraction and microcrystalline structure, as demonstrated both in Mössbauer spectroscopy measurements[56] and ^{229}Th-doped CaF_2 crystals[44]. Single-crystal $^{232}ThF_4$ substrates[45] can potentially be used for epitaxial $^{229}ThF_4$ film growth.

In the future, the quenching of the isomer excited state in a thin film can also be used for constructing a nuclear clock based on internal conversion electrons[57] with comparable performance to clocks based on fluorescence photons. The ThF_4 thin film can be converted to other chemical forms, such as ThO_2 with a cubic lattice structure (Methods), for investigation of the quenching effect and for building a conversion-electron-based clock. The electron escape probability from a ThO_2 thin film may limit the detection efficiency and needs to be studied.

In summary, we address the challenge in the fabrication of solid-state nuclear clocks by demonstrating VUV nuclear spectroscopy of the ^{229}Th clock transition in $^{229}ThF_4$ thin films grown by miniaturized radioactive PVD. Based on detailed DFT calculations, we predict the performance of a $^{229}ThF_4$ solid-state nuclear clock. Our work lays the foundation for future scalable production and widespread use of low-cost integrated nuclear clocks, towards the promise of a simple, portable frequency reference, by resolving important obstacles of material availability and radioactivity limits.

Online content

Any methods, additional references, Nature Portfolio reporting summaries, source data, extended data, supplementary information, acknowledgements, peer review information; details of author contributions and competing interests; and statements of data and code availability are available at https://doi.org/10.1038/s41586-024-08256-5.

1. Tiedau, J. et al. Laser excitation of the Th-229 nucleus. *Phys. Rev. Lett.* **132**, 182501 (2024).
2. Elwell, R. et al. Laser excitation of the ^{229}Th nuclear isomeric transition in a solid-state host. *Phys. Rev. Lett.* **133**, 013201 (2024).
3. Zhang, C. et al. Frequency ratio of the ^{229m}Th nuclear isomeric transition and the ^{87}Sr atomic clock. *Nature* **633**, 63–70 (2024).
4. Hudson, E. R., Vutha, A. C., Lamoreaux, S. K. & DeMille, D. Investigation of the optical transition in the ^{229}Th nucleus: solid-state optical frequency standard and fundamental constant variation (Poster). In *Proc. XXI International Conference on Atomic Physics* (eds Rozman, M. G. et al.) MO28 (2008).
5. Rellergert, W. G. et al. Constraining the evolution of the fundamental constants with a solid-state optical frequency reference based on the ^{229}Th nucleus. *Phys. Rev. Lett.* **104**, 200802 (2010).

6. Peik, E. & Tamm, C. Nuclear laser spectroscopy of the 3.5 eV transition in Th-229. *Europhys. Lett.* **61**, 181–186 (2003).
7. Campbell, C. J. et al. Single-ion nuclear clock for metrology at the 19th decimal place. *Phys. Rev. Lett.* **108**, 120802 (2012).
8. Flambaum, V. V. Enhanced effect of temporal variation of the fine structure constant and the strong interaction in ^{229}Th. *Phys. Rev. Lett.* **97**, 092502 (2006).
9. Litvinova, E., Feldmeier, H., Dobaczewski, J. & Flambaum, V. Nuclear structure of lowest ^{229}Th states and time-dependent fundamental constants. *Phys. Rev. C* **79**, 064303 (2009).
10. Fuchs, E. et al. Implications of the laser excitation of the Th-229 nucleus for dark matter searches. Preprint at https://arxiv.org/abs/2407.15924 (2024).
11. Caputo, A. et al. On the sensitivity of nuclear clocks to new physics. Preprint at https://arxiv.org/abs/2407.17526 (2024).
12. Beeks, K. et al. Fine-structure constant sensitivity of the Th-229 nuclear clock transition. Preprint at https://arxiv.org/abs/2407.17300 (2024).
13. Jeet, J. et al. Results of a direct search using synchrotron radiation for the low-energy ^{229}Th nuclear isomeric transition. *Phys. Rev. Lett.* **114**, 253001 (2015).
14. Hiraki, T. et al. Controlling ^{229}Th isomeric state population in a VUV transparent crystal. *Nat. Commun.* **15**, 5536 (2024).
15. Tkalya, E. V., Varlamov, V. O., Lomonosov, V. V. & Nikulin, S. A. Processes of the nuclear isomer ^{229m}Th(3/2$^+$, 3.5 ± 1.0 eV) resonant excitation by optical photons. *Phys. Scr.* **53**, 296–299 (1996).
16. Tkalya, E. V. Proposal for a nuclear gamma-ray laser of optical range. *Phys. Rev. Lett.* **106**, 162501 (2011).
17. von der Wense, L. & Seiferle, B. The ^{229}Th isomer: prospects for a nuclear optical clock. *Eur. Phys. J. A* **56**, 277 (2020).
18. Beeks, K. et al. The thorium-229 low-energy isomer and the nuclear clock. *Nat. Rev. Phys.* **3**, 238–248 (2021).
19. Peik, E. et al. Nuclear clocks for testing fundamental physics. *Quantum Sci. Technol.* **6**, 034002 (2021).
20. Kazakov, G. A. et al. Performance of a ^{229}Thorium solid-state nuclear clock. *New J. Phys.* **14**, 083019 (2012).
21. Hogle, S. et al. Reactor production of thorium-229. *Appl. Radiat. Isot.* **114**, 19–27 (2016).
22. Forsberg, C. & Lewis, L. *Uses For Uranium-233: What Should Be Kept For Future Needs?* (Oak Ridge National Laboratory, 1999).
23. Jeet, J. *Search for the Low Lying Transition in the ^{229}Th Nucleus.* PhD thesis, Univ. California (2018).
24. Beeks, K. et al. Growth and characterization of thorium-doped calcium fluoride single crystals. *Sci. Rep.* **13**, 3897 (2023).
25. Rellergert, W. G. et al. Progress towards fabrication of ^{229}Th-doped high energy band-gap crystals for use as a solid-state optical frequency reference. *IOP Conf. Ser. Mater. Sci. Eng.* **15**, 012005 (2010).
26. Sletten, G. Preparation of targets of alpha-radioactive isotopes. *Nucl. Instrum. Methods* **102**, 465–468 (1972).
27. Adair, H. L. Preparation and characterization of radioactive samples for various areas of research. *Nucl. Instrum. Methods* **167**, 45–53 (1979).
28. Glover, K. M. et al. The preparation of stable and actinide nuclide targets for nuclear measurements. *IEEE Trans. Nucl. Sci.* **28**, 1593–1596 (1981).
29. Maier, H. J. Preparation of nuclear accelerator targets by vacuum evaporation. *IEEE Trans. Nucl. Sci.* **28**, 1575–1583 (1981).
30. Maier, H. J., Grossmann, R. & Friebel, H. U. Radioactive targets for nuclear accelerator experiments. *Nucl. Instrum. Methods Phys. Res. B* **56**, 926–932 (1991).
31. Greene, J. P., Ahmad, I. & Thomas, G. E. Radioactive targets and source development at Argonne National Laboratory. *Nucl. Instrum. Methods Phys. Res. A* **334**, 101–110 (1993).
32. Baumeister, P. W. *Properties of Multilayer Filters* (Institute of Optics, Univ. Rochester, 1973).
33. IAEA. *Regulations for the Safe Transport of Radioactive Material*. Report No. SSR-6 (Rev. 1) (IAEA, 2018).
34. Jain, A. et al. Commentary: the materials project: a materials genome approach to accelerating materials innovation. *APL Mater.* **1**, 011002 (2013).
35. Ellis, J. K., Wen, X.-D. & Martin, R. L. Investigation of thorium salts as candidate materials for direct observation of the ^{229m}Th nuclear transition. *Inorg. Chem.* **53**, 6769–6774 (2014).
36. Gouder, T. et al. Measurements of the band gap of ThF_4 by electron spectroscopy techniques. *Phys. Rev. Res.* **1**, 033005 (2019).
37. Osipenko, M. et al. Measurement of photo- and radio-luminescence of thin ThF_4 films. *Nucl. Instrum. Methods Phys. Res. A* **1068**, 169744 (2024).
38. Urbach, H. P. & Rikken, G. L. Spontaneous emission from a dielectric slab. *Phys. Rev. A* **57**, 3913–3930 (1998).
39. Dicke, R. H. Coherence in spontaneous radiation processes. *Phys. Rev.* **93**, 99–110 (1954).
40. Liao, W.-T., Das, S., Keitel, C. H. & Pálffy, A. Coherence-enhanced optical determination of the ^{229}Th isomeric transition. *Phys. Rev. Lett.* **109**, 262502 (2012).
41. Karpeshin, F. F. & Trzhaskovskaya, M. B. A proposed solution for the lifetime puzzle of the ^{229m}Th$^+$ isomer. *Nucl. Phys. A* **1010**, 122173 (2021).
42. Kroemer, H. Problems in the theory of heterojunction discontinuities. *CRC Crit. Rev. Solid State Sci.* **5**, 555–564 (1975).
43. Brillson, L. J. *Surfaces and Interfaces of Electronic Materials* (Wiley, 2012).
44. Beeks, K. et al. Optical transmission enhancement of ionic crystals via superionic fluoride transfer: growing VUV-transparent radioactive crystals. *Phys. Rev. B* **109**, 094111 (2024).
45. Pastor, R. & Arita, K. Preparation and crystal growth of ThF_4. *Mater. Res. Bull.* **9**, 579–583 (1974).
46. Martel, L. et al. Insight into the crystalline structure of ThF_4 with the combined use of neutron diffraction, ^{19}F magic-angle spinning-NMR, and density functional theory calculations. *Inorg. Chem.* **57**, 15350–15360 (2018).
47. Bemis, C. E. et al. Coulomb excitation of states in ^{229}Th. *Phys. Scr.* **38**, 657–663 (1988).
48. Gerstenkorn, S. et al. Structures hyperfines du spectre d'étincelle, moment magnétique et quadrupolaire de l'isotope 229 du thorium. *J. Phys.* **35**, 483–495 (1974).
49. Campbell, C., Radnaev, A. & Kuzmich, A. Wigner crystals of ^{229}Th for optical excitation of the nuclear isomer. *Phys. Rev. Lett.* **106**, 223001 (2011).
50. Thielking, J. et al. Laser spectroscopic characterization of the nuclear-clock isomer ^{229m}Th. *Nature* **556**, 321–325 (2018).
51. Yamaguchi, A. et al. Laser spectroscopy of triply charged ^{229}Th isomer for a nuclear clock. *Nature* **629**, 62–66 (2024).
52. Jackson, R. A., Amaral, J. B., Valerio, M. E. G., Demille, D. P. & Hudson, E. R. Computer modelling of thorium doping in $LiCaAlF_6$ and $LiSrAlF_6$: application to the development of solid state optical frequency devices. *J. Phys. Condens. Matter* **21**, 325403 (2009).
53. Pimon, M., Grüneis, A., Mohn, P. & Schumm, T. Ab-initio study of calcium fluoride doped with heavy isotopes. *Crystals* **12**, 1128 (2022).
54. Ludlow, A. D., Boyd, M. M., Ye, J., Peik, E. & Schmidt, P. O. Optical atomic clocks. *Rev. Mod. Phys.* **87**, 637–701 (2015).
55. Röhlsberger, R., Schlage, K., Sahoo, B., Couet, S. & Rüffer, R. Collective Lamb shift in single-photon superradiance. *Science* **328**, 1248–1251 (2010).
56. Dornow, V. A., Binder, J., Heidemann, A., Kalvius, G. M. & Wortmann, G. Preparation of narrow-line sources for the 6.2 keV Mössbauer resonance of ^{181}Ta. *Nucl. Instrum. Methods* **163**, 491–497 (1979).
57. von der Wense, L. & Zhang, C. Concepts for direct frequency-comb spectroscopy of ^{229m}Th and an internal-conversion-based solid-state nuclear clock. *Eur. Phys. J. D* **74**, 146 (2020).
58. Chastain, J. & King R. C. in *Handbook of X-ray Photoelectron Spectroscopy* Vol. 40 (ed. Chastain, J.) 221 (Perkin-Elmer, 1992).

Methods

Verifying the VUV indices of refraction

Because of the dearth of data on indices of refraction in the VUV, it is useful to verify the values obtained from the literature. To do this, samples of the various materials used in our experiment were placed at normal incidence in our VUV beamline to measure their transmission at about 148.38 nm.

The literature values for the refractive indices of MgF_2 (ref. 59) are 1.4828 (O-ray) and 1.4977 (E-ray), whereas the value for Al_2O_3 is 2.32(2), which is obtained by averaging various analyses found in ref. 60. A thin sample of MgF_2 (250 μm) was found to have 91(4)% transmission, whereas a thin sample of Al_2O_3 (175 μm) has 61(9)% transmission. Assuming no additional absorption and normal Fresnel reflection losses, this is consistent with values of refractive indices of $n = 1.55(17)$ for MgF_2 and $n = 2.77(41)$ for Al_2O_3. Thus, our transmission measurements are in agreement with the literature values of the indices of refraction assuming no additional absorption in the thin samples.

Obtaining the literature values for the VUV refractive index of ThF_4 is more challenging as very few data are available. Extrapolating the measurements taken in ref. 32 to 148.38 nm leads to a prediction of $n = 1.82$ for ThF_4. As the index of refraction typically rises in the VUV as the band edge of the material is approached, this value is probably a lower bound. Therefore, we also performed a rudimentary measurement of n_{ThF_4} by comparing the amount of 148.38 nm light transmitted through a 5-mm thick sample of MgF_2 that was uncoated and coated with a thin $^{229}ThF_4$ film. By assuming no absorption in the thin $^{229}ThF_4$ film and normal Fresnel reflections at the interfaces, a value of $n_{ThF_4} = 1.95(30)$ was obtained.

Calculation of the system detection efficiency

The system detection efficiency consists of two main components: the efficiency with which a photon emitted from the decay of the isomer is collected by our detectors and the quantum efficiency (QE) of the detectors. The QE of our photomultiplier tube (PMT) detectors (Hamamatsu model R6835) was provided by the calibrations of the manufacturer (about 12% at 148 nm).

The collection efficiency is calculated from custom ray-tracing software. This program accounts for refraction and multiple reflections in the ThF_4-substrate system to provide an accurate distribution of rays emerging from the sample. Given that the $^{229}ThF_4$ samples are inhomogeneous in thickness, we make the approximation that interference effects are negligible. The efficiency with which rays emerge from the Al_2O_3 substrate towards the PMT is about 7.6% and the MgF_2 substrate towards the PMT is around 8.6%. The calculated ray distributions from the sample into the vacuum are passed to commercial ray-tracing software to determine the number of rays that ultimately reach the detectors[61], which was about 72% for both substrates. As such, the total system detection efficiency was about 0.7% for both substrates.

Signal detection and backgrounds

The output waveform pulses from the R6835 PMT are amplified through a Stanford Research Systems SR445A preamplifier before being routed to the waveform digitizer. The digitizer is set to trigger at about 25% pulse amplitude and has an approximately 8 ns dead time between waveform acquisitions. In both $^{229}ThF_4$ targets on Al_2O_3 and MgF_2, the total number of detected signal photons from the nuclear isomer decay was of the order of about 2×10^4 (varying with laser power), whereas the backgrounds were around 9,000 counts per second (cps) for Al_2O_3 and 1,300 cps for MgF_2.

Additional $^{229}ThF_4$ thin film properties

The ^{229}Th activity of both $^{229}ThF_4$ targets used in the nuclear laser spectroscopy was measured to be about 21 kBq, corresponding to approximately 7.5×10^{15} ^{229}Th nuclei. We use the known activity of ^{229}Th (1.68×10^{12} Bq mol^{-1}), the density of $^{229}ThF_4$ (6.3 g cm^{-3}) and the diameter of the target (about 5 mm) to roughly estimate the thickness of the films. The thickness obtained is approximately 30 nm. This is in agreement with profilometer and AFM measurement results for different targets, scaled by their radioactivity.

Thin film targets created by vapour deposition tend to be amorphous. We performed preliminary studies of the thin film structure using grazing-incidence wide-angle scattering X-ray diffraction. The correlation length, which is an estimation of the average grain size, is extracted using the Scherrer equation[62] to be about 30 Å for a similarly produced $^{232}ThF_4$ sample. In future studies, X-ray diffraction measurements in combination with VUV nuclear spectroscopy will help characterize the $^{229}ThF_4$ nuclear transition sensitivity to the sample crystallinity.

DFT calculations

The DFT calculations were performed using the PBE (Perdew, Burke, Ernzerhof) functional and the projector augmented wave method as implemented in the Vienna Ab initio Simulation Package (VASP), v.6.4.2 (refs. 63–65). The calculations were done on the primitive cell of ThF_4, which contains six formula units. All calculations used a 500-eV plane wave cut-off and a Γ-centred k-mesh with a k-point spacing of 0.03 Å^{-1} (4-4-5 for the primitive unit cell). The structure (atomic positions and lattice parameters) of ThF_4 was optimized until the force components on all atoms were less than 0.02 eV Å^{-1}. The EFGs were computed using the method implemented in VASP[66]. Convergence tests with respect to plane wave cut-off and SCF (self-consistent field) convergence criterion were performed up to 800 eV and 10^{-8} eV, respectively. The tests showed that settings of 500 eV and 10^{-5} eV, used in all our calculations, were sufficient to converge the EFGs.

A single-point calculation with the HSE06 hybrid functional[67] was used to confirm the accuracy of the computed EFGs. The parameters for the first site are $V_{zz} = 309.3$ V Å^{-2} and $\eta = 0.428$ and for the second site $V_{zz} = 308.1$ V Å^{-2} and $\eta = 0.194$, matching the PBE results very well. This calculation used the same computational settings as above except that a 4-4-4 k-mesh was used with a downsampling factor of 2 for the Fock operator. The band gap computed with HSE06 was 8.85 eV, consistent with previous calculations[35].

Nuclear transition quenching in thin films

Our measured lifetime of about 160 s of the ^{229m}Th isomeric excited state in $^{229}ThF_4$ films is significantly shorter than the ^{229m}Th lifetime of about 600 s measured in doped crystals[1,2]. The nuclear lifetime can be affected by multiple factors and quenching mechanisms.

The bare ^{229m}Th isomer predominantly decays to its ground state by magnetic-dipole (M1) radiation. The corresponding vacuum isomer lifetime is $\tau_{is} \sim 1{,}900$–$2{,}500$ s (refs. 1,2,51,68). The ^{229}Th nucleus in ThF_4, however, is embedded into the electronic cloud of Th^{4+} ion and the ion itself into the crystal lattice. The M1 decay rate can be modified by the host environment and new, competing, decay channels may open up.

It should be noted that if a quantum emitter is embedded into a bulk non-magnetic dielectric with refractive index n, its M1 decay rate is increased by a factor of n^3 compared with its vacuum value A_{M1}^{vac} (refs. 69,70). The M1 radiative lifetime becomes shorter in a dielectric because of photon mode field renormalization and the change in the photon density of states. This is an accepted explanation for the shortened isomer lifetime in doped crystals[1,2] compared with its vacuum (bare nucleus) value[51]. In our experiment, however, $^{229}ThF_4$ comes as a film deposited on a substrate. The substrate–film and vacuum–film interfaces modify the allowed photon modes and, therefore, the coupling and the photonic density of states. This influences both the emission rate and angular distribution[38,71]. Following ref. 38, we quantized electromagnetic fields in our experimental geometry. We find that the ^{229}Th M1 rate can be parameterized as $A_{M1}(\mathbf{r}) = g(\mathbf{r})A_{M1}^{vac}$, where the position-dependent M1 Purcell factor $g(\mathbf{r})$ scales the vacuum A_{M1}^{vac} rate.

For a bulk dielectric with refractive index n, $g(\mathbf{r}) = n^3$. The M1 Purcell factor for non-magnetic media is continuous across interfaces. Therefore, $g(\mathbf{r})$ in a thin film ($d \ll \lambda/n_{ThF_4}$) must smoothly interpolate between the bulk substrate value n_{sub}^3 and the vacuum value of 1. Thus, the M1 decay rate depends on how deep a ^{229}Th nucleus is in the film, and an experiment would not observe a single exponential decay. Moreover, the rate would depend on the substrate refractive index. In the opposite limit of thick films, we find that $g(\mathbf{r}) \approx n_{ThF_4}^3$ and is largely position and substrate independent, resulting in a single exponential decay; this is consistent with data in Fig. 2c. Moreover, our measured decay rates for $^{229}ThF_4$ are indistinguishable for decay on the MgF_2 and Al_2O_3 substrates, whereas these two substrates have substantially different refractive indexes. We conclude that the Purcell effect due to the substrates does not have a leading order role in determining the isomer lifetime in our experiments.

The emitter lifetime can be also shortened by collective coherent effects such as superradiance[39,40]. These seem unlikely, because the thorium number density per wavelength cubed, $(\lambda/n_{ThF_4})^3\rho_{Th} > 10^6$, is reduced by the inhomogeneous broadening[5], $\Gamma_{nat}/\Gamma_{inh} < (1/150)$ s/$(2\pi \times 1\,\mathrm{kHz}) = 10^{-6}$ and the participation factor, $p = 10^{-3}$.

Other explanations for the shorter isomer lifetime observed here include a large index of refraction for ThF_4 and quenching by the host material.

Explaining the observed lifetime as a consequence of the $^{229}ThF_4$ refractive index requires $n_{ThF_4} = \sqrt[3]{\tau_{is}/\tau} = 2.2 - 2.5$, given the vacuum isomer lifetime $\tau_{is} \approx 1{,}800$–$2{,}500$ s (refs. 1,2). To our knowledge, the shortest wavelength measurement of n_{ThF_4} is about 157 nm (ref. 32). Linearly extrapolating this result to 148 nm predicts $n_{ThF_4} = 1.82$; this estimate is probably a lower bound as the index of refraction of a material typically rises markedly in the VUV. To provide an additional estimate of n_{ThF_4} at 148 nm, we measured and compared the transmission of our laser through a $^{229}ThF_4$-coated MgF_2 substrate to that of an uncoated MgF_2 substrate. Assuming the transmission is determined solely by the Fresnel reflection at the interfaces, this measurement suggests $n_{ThF_4} = 1.95(30)$. Although this value is close to the n_{ThF_4} inferred from the isomeric lifetime, it may not fully explain the observed lifetime.

A new electric-dipole (E1) channel for a nuclear decay in a solid-state environment has been pointed out in ref. 2. This decay mechanism is enabled by hybridization of electronic states by the crystal fields. The hyperfine interaction couples the nuclear degree of freedom to these mixed-parity electronic states, enabling a competing E1 decay channel for the isomeric state. Qualitatively, in thin $^{229}ThF_4$ films, the mixing of opposite-parity electronic states can be further enhanced by electric fields generated because of internal mechanical strains. Interface between $^{229}ThF_4$ and the substrate can also generate large mixing electric fields: (1) lattice mismatch at the interface can cause strains[43], and (2) when two dissimilar insulators are brought into contact, their Fermi levels must align causing band bending and space charge and dipole layer formation[42,43].

Apart from the enumerated quenching mechanisms, the nuclear transition lifetime may be affected by the bulk and surface impurities and stray surface charges.

Although the observed shorter isomer lifetime is not yet fully understood, it also offers a rich landscape for exploration at the interface of nuclear and solid-state physics and quantum optics, potentially leading to new insights in these fields. This will be the subject of future studies.

Zeeman sensitivities of the nuclear states

The nuclear energy levels are described by the Hamiltonian:

$$\hat{H} = -\mu_\alpha \mathbf{I}\cdot\mathbf{B} + \frac{eQ_\alpha V_{zz}}{4I(2I-1)}[3\hat{I}_z^2 - \hat{I}^2 + \eta(\hat{I}_x^2 - \hat{I}_y^2)], \quad (2)$$

where $\hat{I}$ is the total nuclear spin operator, $\hat{I}_{x,y,z}$ are the component of the nuclear spin operators, $\eta = |V_{xx} - V_{yy}|/|V_{zz}|$ is the EFG asymmetry parameter and $\alpha = \{g, e\}$ denotes the ground and excited nuclear states, respectively, which is parameterized by $Q_g = 3.149(3)$ eb (ref. 47), $\mu_g = 0.360(7)\mu_N$ (refs. 48,49), $Q_e = 1.77(2)$ eb (ref. 51) and $\mu_e = -0.378(8)\mu_N$ (ref. 51), where μ_N is the nuclear magneton.

ThF_4 hosts ^{229}Th in two non-equivalent sites. The first site (type 1), shown as orange spheres in Fig. 3a, experiences a crystal EFG of $V_{zz} = 310.5$ V Å^{-2} and $\eta = 0.437$ and is twice as populated as the second site (type 2), shown as red spheres in Fig. 3a, which experiences a crystal EFG of $V_{zz} = 308.9$ V Å^{-2} and $\eta = 0.194$. Owing to the differing EFGs, these two sites have non-degenerate energy levels (Fig. 3b) and therefore distinct laser spectra as shown in Fig. 3b.

To calculate the expected linewidth of the various ^{229}Th nuclear transitions, we perform a Monte Carlo simulation as follows. First, it is assumed that the nuclear spin of each ^{19}F and ^{229}Th atom is randomly oriented and the magnetic field due to these magnetic dipoles created at the central thorium nucleus is calculated. For this calculation, the structure shown in Fig. 3a is extended to include about 500 atoms to ensure convergence. This process is repeated 10,000 times to create a sample of possible magnetic fields at the central thorium nucleus. Next, the Hamiltonian above is numerically diagonalized for both $I = 5/2$ and $I = 3/2$ states at each sample of the magnetic field and the shift in transition frequency is found. The average and the standard deviation of the sample of transition frequency shifts are found. The average shift is approximately zero, as expected because the EFG defines the quantization axis, whereas the standard deviation, which should be a reasonable estimate of the transition linewidth, is shown in Extended Data Table 1.

Conversion from fluoride to oxide

As mentioned in the main text, a $^{229}ThO_2$ thin film is desirable for its cubic symmetry leading to vanishing electric quadrupole splitting as well as for constructing a conversion-electron-based nuclear clock because of its low bandgap[57]. We have developed a procedure for reliably converting a $^{229}ThF_4$ thin film to $^{229}ThO_2$ using pyrohydrolysis.

For the conversion, the $^{229}ThF_4$ target is placed on a hot plate (Corning, PC-420D) set to a temperature of 550 °C. Argon gas is saturated with water by being sent through a water-filled bubbler and is flowed through a glass tube positioned directly over the target. Moreover, a 300 W halogen lamp (Omnilux ELH, 120 V) is placed a few centimetres from the target to further increase the surface temperature. The process is terminated after about 1 h, although significantly shorter reaction times might be sufficient. Under these conditions, the fluoride layer converts to oxide following the reaction

$$ThF_4 + 2H_2O \rightarrow ThO_2 + 4HF.$$

It was a concern that the surface layer might disintegrate during the process of pyrohydrolysis and that the oxide layer might not stay attached to the substrate. However, no such problems occurred. However, shrinking of the layer thickness, as expected for stoichiometric reasons, did occur and was confirmed by AFM measurements. The chemical composition of the target was also confirmed as $^{229}ThO_2$ through XPS. Notably, pyrohydrolysis is a very aggressive process, potentially also leading to the oxidation of the substrate. The laser excitation of a $^{229}ThO_2$ thin film, possibly observed by monitoring conversion electrons[57], has yet to be demonstrated and will be the subject of future studies.

Determination of clock stability

We estimate the clock stability as[72]

$$\sigma = \frac{1}{2\pi QS}\sqrt{\frac{T_e + T_c}{\tau}},$$

where $Q = f_0/\Delta f$ is the transition quality factor, S is the signal-to-noise ratio (SNR), T_e is the excitation time, T_c is the fluorescence collection

time and τ is the averaging time. We assume the clock is driven on the $|5/2, \pm 1/2\rangle \leftrightarrow |3/2, \mp 1/2\rangle$ transition and use the calculated Δf in Extended Data Table 1. For our analysis, we assume $T_e = T_c = 200$ s, and an SNR given by

$$S = \frac{N_d}{\sqrt{N_d + N_b}},$$

where $N_b = b \times T_c$ is the total background counts, $b = 6 \times 10^4$ cps (based on the MgF_2 substrate background and scaling from a 20 nm to a 100 nm film), and N_d is the number of detected photons from the thorium isomer decay given by

$$N_d = \eta N_e (1 - e^{-\Gamma T_c}),$$

where N_e (about 2.7×10^{11}) is the total number of ^{229}Th nuclei excited, $\eta = 0.01$ is the assumed system detection efficiency and Γ is the transition decay rate. N_e is calculated assuming that the probe laser linewidth is significantly smaller than the inhomogeneous Zeeman-limited transition linewidth, the probe laser power is 1 μW and all quenching mechanisms have been suppressed so that the maximum emitter fraction is achieved. From this we obtain a projected clock performance of $5 \times 10^{-17}/\sqrt{\tau}$.

Data availability

The data that support the findings of this study are available from the corresponding author upon request.

59. Li, H. H. Refractive index of alkaline earth halides and its wavelength and temperature derivatives. *J. Phys. Chem. Ref. Data* **8**, 161–290 (1980).
60. French, R. H., Müllejans, H. & Jones, D. J. Optical properties of aluminum oxide: determined from vacuum ultraviolet and electron energy-loss spectroscopies. *J. Am. Ceram. Soc.* **81**, 2549–2557 (1998).
61. Zemax OpticStudio. Zemax v.12.2 (ANSYS Inc., 2012).
62. Steele, J. A. et al. How to GIWAXS: grazing incidence wide angle X-ray scattering applied to metal halide perovskite thin films. *Adv. Energy Mater.* **13**, 2300760 (2023).
63. Kresse, G. & Furthmuller, J. Efficient iterative schemes for *ab initio* total-energy calculations using a plane-wave basis set. *Phys. Rev. B* **54**, 11169–11186 (1996).
64. Perdew, J. P., Burke, K. & Ernzerhof, M. Generalized gradient approximation made simple. *Phys. Rev. Lett.* **77**, 3865–3868 (1996).
65. Blöchl, P. E. Projector augmented-wave method. *Phys. Rev. B* **50**, 17953–17979 (1994).
66. Petrilli, H. M., Blochl, P. E., Blaha, P. & Schwarz, K. Electric-field-gradient calculations using the projector augmented wave method. *Phys. Rev. B* **57**, 14690–14697 (1998).
67. Krukau, A., Vydrov, O., Izmaylov, A. & Scuseria, G. Influence of the exchange screening parameter on the performance of screened hybrid functionals. *J. Chem. Phys.* **125**, 224106 (2006).
68. Kraemer, S. et al. Observation of the radiative decay of the ^{229}Th nuclear clock isomer. *Nature* **617**, 706–710 (2023).
69. Nienhuis, G. & Alkemade, C. Th. J. Atomic radiative transition probabilities in a continuous medium. *Physica B+C* **81C**, 181–188 (1976).
70. Tkalya, E. V. Spontaneous emission probability for M1 transition in a dielectric medium: ^{229m}Th($3/2^+$, 3.5±1.0 eV) decay. *JETP Lett.* **71**, 311–313 (2000).
71. Lukosz, W. & Kunz, R. E. Light emission by magnetic and electric dipoles close to a plane dielectric interface. II. Radiation patterns of perpendicular oriented dipoles. *J. Opt. Soc. Am.* **67**, 1615–1619 (1978).
72. Boyd, M. M. *High Precision Spectroscopy of Strontium in an Optical Lattice: Towards a New Standard for Frequency and Time.* PhD thesis, Univ. Colorado (2007).

Acknowledgements We acknowledge funding support from the Army Research Office (W911NF2010182), the Air Force Office of Scientific Research (FA9550-19-1-0148), the National Science Foundation QLCI OMA-2016244, the National Science Foundation PHY-2317149, and the National Institute of Standards and Technology. J.S.H. acknowledges support from the National Research Council Postdoctoral Fellowship. L.v.d.W. acknowledges funding from the Humboldt Foundation through a Feodor Lynen fellowship. We thank the National Isotope Development Center of DOE and the Oak Ridge National Laboratory for providing the Th-229 used in this work. This work was also supported in part by NSF awards PHYS-2013011, PHYS-2412982, PHY-2207546 and PHY-2412982, and ARO award W911NF-11-1-0369. E.R.H. acknowledges institutional support by the NSF QLCI Award OMA-2016245. This work used Bridges-2 at Pittsburgh Supercomputing Center through allocation PHY230110 from the Advanced Cyberinfrastructure Coordination Ecosystem: Services and Support (ACCESS) programme, which is supported by the National Science Foundation grants 2138259, 2138286, 2138307, 2137603 and 2138296. We thank C. E. Düllmann and D. Renisch for their discussions; J. Lin and D. V. Reddy for proofreading; A. S. Cavanagh, J. C. Beimborn, K. Hagen, J. MacLennan, V. Martinez, M. Ashton, B. C. Denton, M. R. Statham and L. Deison for technical assistance. We acknowledge the use of the Materials Research X-Ray Diffraction Facility at the University of Colorado Boulder (RRID: SCR_019304), with instrumentation supported by NSF MRSEC grant DMR-1420736.

Author contributions C.Z., L.v.d.W., J.F.D., J.S.H., T.O., H.U.F. and J.Y. produced and characterized the sample. R.E., J.E.S.T. and E.R.H. performed the laser spectroscopy measurement. H.W.T.M., A.N.A., H.B.T.T. and A.D. performed theory calculations. All authors wrote the paper.

Competing interests The authors declare no competing interests.

Additional information

Supplementary information The online version contains supplementary material available at https://doi.org/10.1038/s41586-024-08256-5.

Correspondence and requests for materials should be addressed to Jun Ye or Eric R. Hudson.

Peer review information *Nature* thanks Mikhail Osipenko and the other, anonymous, reviewer(s) for their contribution to the peer review of this work. Peer reviewer reports are available.

Extended Data Table 1 | Estimated linewidths of the allowed M1 transitions

$\|3/2, \text{“}m_I\text{”}\rangle$	$\|5/2, \text{“}m_I\text{”}\rangle$	$\Gamma/(2\pi)$ kHz (Type 1)	$\Gamma/(2\pi)$ kHz (Type 2)
$\pm 3/2$	$\pm 5/2$	6.5	6.5
$\pm 3/2$	$\pm 3/2$	5.4	5.1
$\pm 3/2$	$\pm 1/2$	6.1	6.1
$\pm 1/2$	$\pm 3/2$	5.7	5.3
$\pm 1/2$	$\pm 1/2$	6.8	6.9
$\pm 1/2$	$\mp 1/2$	1.3	1.1